International Journal of Thermophysics, Vol. 28, No. 2, April 2007 (© 2007)
DOI: 10.1007/s10765-007-0196-9

Johnson Noise Thermometry near the Zinc Freezing Point Using Resistance-Based Scaling

W. L. Tew,[1,2] J. R. Labenski,[1] S. W. Nam,[3] S. P. Benz,[4] P. D. Dresselhaus,[4] and C. J. Burroughs[4]

Johnson noise thermometry (JNT) is a primary method of measuring temperature which can be applied over wide ranges. The National Institute of Standards and Technology (NIST) is currently using JNT to determine the deviations of the International Temperature Scale of 1990 (ITS-90) from the thermodynamic temperature in the range of 505–933 K, overlapping the ranges of both acoustic gas-based and radiation-based thermometry. Advances in digital electronics have now made viable the computationally intensive and data-volume-intensive processing required for JNT using noise-voltage correlation in the frequency domain. The spectral noise power, and consequently the thermodynamic temperature T, of a high-temperature JNT probe is determined relative to a known reference spectrum using a switched-input digital noise-voltage correlator and simple resistance-scaling relationships. Comparison of the JNT results with standard platinum resistance thermometers calibrated on the ITS-90 gives the deviation of the thermodynamic temperature from the temperature on the ITS-90, $T - T_{90}$. Statistical uncertainties under $50\,\mu\mathrm{K}\cdot\mathrm{K}^{-1}$ are achievable in less than 1 day of integration by fitting the effects of transmission-line time constants over bandwidths of 450 kHz. The methods and results in a 3 K interval near the zinc freezing point ($T_{90-\mathrm{ZnFP}} \equiv 692.677\,\mathrm{K}$) are described. Preliminary results show agreement between the JNT-derived temperatures and the ITS-90.

KEY WORDS: ITS-90; Johnson noise; noise thermometry; temperature.

[1] Process Measurements Division, National Institute of Standards and Technology, 100 Bureau Drive, Gaithersburg, Maryland 20899, U.S.A.
[2] To whom correspondence should be addressed. E-mail: wtew@nist.gov
[3] Optoelectronics Division, National Institute of Standards and Technology, 325 Broadway, Boulder, Colorado 80303, U.S.A.
[4] Quantum Electrical Metrology Division, National Institute of Standards and Technology, 325 Broadway, Boulder, Colorado 80303, U.S.A.

1. INTRODUCTION

The International Temperature Scale of 1990 (ITS-90) is an artifact-based temperature scale designed to approximate thermodynamic temperature [1]. The existence of thermodynamic errors in the ITS-90 has been known since its adoption, but these have only recently been quantified by primary thermodynamic methods such as acoustic gas thermometry for temperatures $T < 510\,\mathrm{K}$ [2] and radiance-based methods [3] for $T > 730\,\mathrm{K}$. Johnson noise thermometry (JNT) is another primary method which has been applied over a range $0.006\,\mathrm{K} < T < 1{,}826\,\mathrm{K}$ and which is capable of achieving uncertainties that are competitive with radiance-based techniques [4].

The power spectral density S of voltage fluctuations originating from Johnson noise in a conductor of resistance R in equilibrium at temperature T is approximated by

$$S = 4k_{\mathrm{B}} T R, \tag{1}$$

to within $1\,\mu\mathrm{K}\cdot\mathrm{K}^{-1}$ over the frequencies of interest, and k_{B} is the Boltzmann constant. Most JNT measurement systems switch between two noise source inputs, '1' and '2', in an alternating fashion so that an unknown source of spectral power density S_1 may be compared with some known reference source of spectral density S_2 (see Fig. 1). When the reference noise source is the Johnson noise from another conductor at a known temperature T_2, adjusted such that $S_2 \approx S_1$, then the measurement problem reduces to that of scaling the temperatures by the inverse resistance ratio or,

$$\frac{T_1}{T_2} = \frac{S_1}{S_2}\frac{R_2}{R_1}. \tag{2}$$

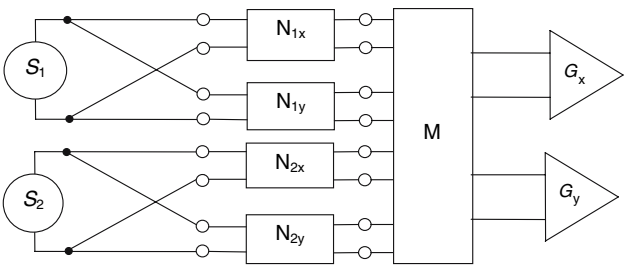

Fig. 1. Network representation of inputs to the noise-voltage comparator with parallel channels x and y, sources S_1 and S_2, switching network M, and coupling networks $\mathrm{N}_{i\mathrm{x}}$ and $\mathrm{N}_{i\mathrm{y}}$.

Equation (2) is in fact only an idealization, and frequency-dependent corrections are always necessary due to finite time constants associated with both the unknown input and the reference input. In general, the time constants are different for the two inputs resulting in different frequency dependences for S_1 and S_2 and hence a frequency-dependent ratio spectrum (S_1/S_2). Such differences are unavoidable using resistance-based scaling methods where the source impedances of R_1 and R_2 are deliberately mismatched, and the degree of this mismatch increases as the temperature ratio T_1/T_2 increases. The time constants τ are those which naturally arise from series and parallel combinations of the source impedances, the pre-amplifier input impedance, and other impedances associated with the input coupling networks (N_{ix} and N_{iy} in Fig. 1; $i = 1, 2$) in-between [5]. The time-constant mismatch imposes a requirement that S_1/S_2 be determined in the low-frequency limit of $2\pi f\tau \ll 1$ or, equivalently, making the substitution of $\lim_{f\to 0} \frac{S_1}{S_2}$ into Eq. (2). Hence, one of the main challenges of JNT is to account for, or to some extent compensate for, the differences in these time constants.

Another challenge specific to JNT is the long integration time t_{int} required to achieve a given relative statistical precision $u_r(S)$ as given by

$$u_r(S) = \frac{1}{\sqrt{2t_{\text{int}}\Delta f_c}} \left[1 + \left(\frac{\overline{S_C} + \overline{S_N}}{\overline{S_C}} \right)^2 \right]^{1/2}, \tag{3}$$

where S_C and S_N are the average power spectral densities of the correlated and uncorrelated noise powers, respectively, and Δf_c is the correlation bandwidth [6]. While expanding the measurement bandwidth will increase Δf_c and therefore reduce $u_r(S)$ for a given t_{int}, there is a practical trade-off involved due to accompanying higher-order frequency dependence in the ratio spectrum and the commensurate uncertainty in accounting for those effects [5].

The ITS-90 defines the Zn freezing point $T_{90-\text{ZnFP}} \equiv 692.677\,\text{K}$ based on a compromise between two discrepant gas thermometry data sets available prior to 1990 [7]. We describe our methods and results for JNT measurements over the narrow interval $690\,\text{K} < T_1 < 693\,\text{K}$ as compared directly against standard platinum resistance thermometers (SPRTs) calibrated on the ITS-90.

2. EXPERIMENTAL

Referring to the block diagram of Fig. 2, the experimental system consists of a digital noise-voltage correlator (NVC), a vacuum furnace,

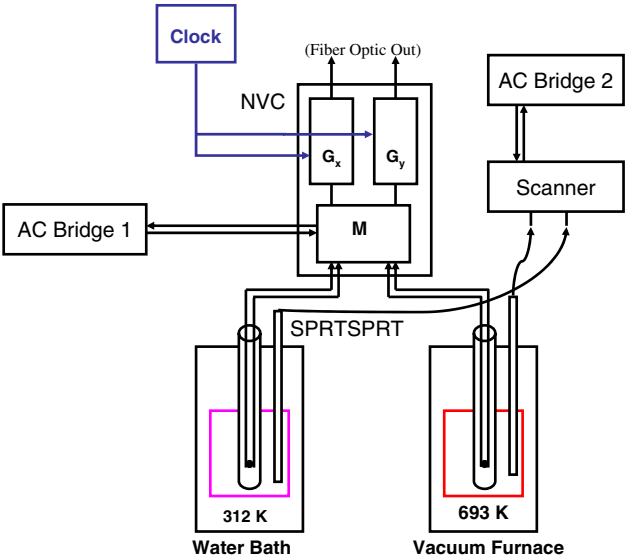

Fig. 2. System block diagram. The noise-voltage correlator (NVC) is connected to each of two noise probes through an internal switching network M. The noise probes are equilibrated with SPRTs in a low-temperature water bath and a high-temperature vacuum furnace.

high-temperature noise probe, SPRTs, a stirred water bath, reference noise probe, and two ac resistance bridges. The noise-voltage correlator is a two-channel, high-gain, over-sampled system using 50 megasample/s digitizers followed by digital signal processors operating on a 50 MHz clock and an output data rate of 2^{21} sample/s. Fast-Fourier-transforms (FFTs) are performed on the time series data to produce the auto-correlation power spectra v_x^2 and v_y^2 for each channel x and y, and the cross-correlation power spectrum $S_C = v_x v_y^*$ between the two channels, where v_y^* is the complex conjugate of the y-channel voltage spectral density. Further details are described elsewhere [8,9].

The vacuum furnace is a three-zone design made from two concentric shells of high-purity copper surrounding a solid copper block where four Ni-alloy thermowells terminate. The vacuum jacket is evacuated at temperature to a pressure $< 10^{-6}$ mbar, closed-off, and held with no active pumping while in use. The two outermost zones are actively controlled via industrial PRTs using direct-current (dc) excitation, while the innermost zone is allowed to passively equilibrate without heating. The two control PRTs are installed in separate smaller thermowells which terminate in

sections of their respective control zones. All heating elements are bi-filar in construction and are driven with linear dc power supplies producing a total applied heating power of less than 100 W.

Two types of SPRTs are used, all are 25 Ω nominal resistance at the water triple point (WTP). Conventional long-stem types with fused-silica sheaths are calibrated at NIST [10] from the WTP to the aluminum freezing point and used continuously in the comparison furnace. The SPRTs are removed from the furnace every 10–20 days to check stability of the WTP resistance. Capsule SPRTs are used for the water bath and other thermal reference systems used for testing. These are calibrated from the WTP to the Ga triple point. Details on the fixed-point materials and construction are found elsewhere [11].

All SPRTs are measured with an ac resistance bridge operating at 90 Hz with a relative standard uncertainty of $\approx 1\,\mu\Omega \cdot \Omega^{-1}$ for resistances $< 100\,\Omega$. A second similar resistance bridge measures the probe resistances with a relative uncertainty of $\approx 2\,\mu\Omega \cdot \Omega^{-1}$ for resistances $< 400\,\Omega$.

The high-temperature noise probes contain two resistance alloy elements made from 50 μm diameter wire in 99.8% purity alumina insulators and trimmed to $\approx 50\,\Omega$ each at 0°C. Elements made from both Ni–Cr and Pt–W alloys have been used, having temperature coefficients of ≈100 and $\approx 280\,\mu\Omega \cdot \Omega^{-1} \cdot \mathrm{K}^{-1}$, respectively. These resistors are connected in the "five-wire" pattern shown in Fig. 3. The high-temperature noise probes have two fused-quartz insulators and Ag lead wires which serve as transmission lines for the noise voltage. The outside surfaces of these insulators are coated with a Pt film conductor which is tied to the common ground.

The reference probes are constructed for service at $T_2 < 370\,\mathrm{K}$ using Teflon and fiber–glass–epoxy-resin composite insulators. The reference resistors are commercial metal-foil types with three terminals which define two adjacent resistors matched in both value ($125 \pm 0.05\,\Omega$) and temperature coefficient ($< 50\,\mu\Omega \cdot \Omega^{-1} \cdot \mathrm{K}^{-1}$). All probes are connected to the

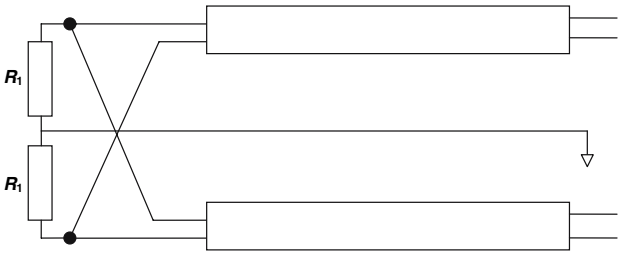

Fig. 3. The high-temperature probe geometry, five-wire connection with fused-quartz insulators.

NVC inputs using shielded-twisted-pair cables made from foam-polyethelene insulation. This insulation has low capacitance ($\approx 87\,\mathrm{pF \cdot m^{-1}}$ pair-to-shield) and low loss tangent ($\tan\delta < 10^{-3}$) over the frequencies of interest here.

All measurement systems are housed in a double-wall shielded room while the computers are kept outside of this room. Both the NVC electronics and the low-frequency measurement systems (e.g., ac bridges) are interfaced with the computers via fiber-optic cables which pass through the walls. We derive all line power in our shielded room from a digitally regenerated UPS system which is synchronized to a local 60 Hz oscillator independent of the utility frequency.

In order to minimize the effects of nonlinearity in the amplifier chain, certain constraints are normally applied in the experimental parameters. The total root-mean-square (rms) voltage V_{rms} in a given channel is the square root of the integrated power spectral density or $\sqrt{\int (S_{\mathrm{C}} + S_{\mathrm{N}})\mathrm{d}f}$ when referred to the input. To a first approximation, the frequency dependence of S_{C} is mediated by a net time constant τ formed by the shunt capacitance and series inductance of the input coupling network and the source resistance via factors of $(1 + (\tau\omega)^2)^{-1/2}$ in the voltage transfer function [5]. In contrast, the uncorrelated channel noise of $S_{\mathrm{N}}^{1/2} \approx 1\,\mathrm{nV} \cdot \mathrm{Hz}^{-1/2}$ is primarily due to the pre-amplifier and filtering components in the amplifier chain with 3 dB corner frequencies $f_{3\,\mathrm{dB}} = 2\,\mathrm{MHz}$. Hence, $V_{\mathrm{rms}} \approx (k_{\mathrm{B}} T R/\tau + V_{\mathrm{N}}^2)^{1/2}$ and the noise voltages of the two inputs will be dissimilar unless $R_1 T_1/\tau_1 = R_2 T_2/\tau_2$. In our measurements we generally impose this condition as two separate constraints, $R_1 T_1 \approx R_2 T_2$ and $\tau_1 \approx \tau_2$, keeping both the low-frequency spectral density and the total rms voltage approximately constant. The time-constant constraint is achieved through the use of compensating capacitors shunting each transmission line conductor to ground. We use the $BaTiO_3$ composite-chip capacitors for this purpose (commonly known as "NPO") which exhibit frequency-independent capacitance and $\tan\delta < 10^{-3}$ over the frequencies of interest and temperature coefficients of $< 30\,\mu\mathrm{F \cdot F^{-1} \cdot K^{-1}}$.

3. RESULTS

The noise power ratio spectra are generated during successive "runs" lasting between 12 and 24 h. Since the size of any possible nonlinearity is not well known, data are generated with varying degrees of time-constant mismatches which determine the sign and magnitude of the frequency roll-off in S_1/S_2. A set of four typical ratio spectra using different degrees of time-constant mismatches are shown superimposed together in Fig. 4

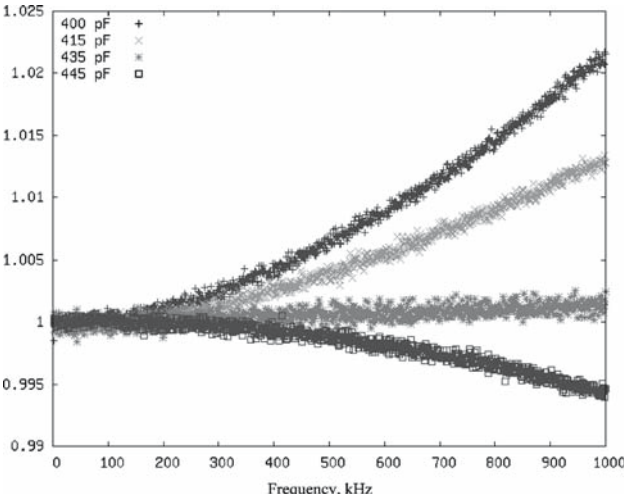

Fig. 4. A sample of four typical ratio spectra with differing degrees of time-constant mismatch. The data are derived by selection of four different values of compensation capacitor sets from 400 to 445 pF for each gate.

extending to 1 MHz, or just below the Nyquist frequency of 2^{20} Hz. In practice, these spectra are fit to simple polynomials in frequency $\sum_i a_i f^i$ using up to third-order terms out to a fitting limit of 450 kHz. This limit was chosen based on our observation that fitting the data beyond that point requires fourth-order terms and higher and the need to keep the total number of necessary fitting parameters to a minimum for optimum statistical precision. We generally produce three separate fits for every data run: (1) a two-parameter fit, $a_0 + a_2 f^2$; (2) a three-parameter fit, $a_0 + a_1 f + a_2 f^2$; and (3) a four-parameter fit, $a_0 + a_1 f + a_2 f^2 + a_3 f^3$. The fit parameter a_0 is then extracted to determine $\lim_{f \to 0} \frac{S_1}{S_2}$ and the temperature according to Eq. (2). Details of the fitting results are given in Ref. 5.

The uncorrected data are summarized in Table I and Fig. 5 in terms of the deviation from ITS-90 temperatures. The statistical uncertainties are based on the standard error estimates for a_0 as derived from the covariance matrix from each fit. The sequence of 20 data runs shown here represents 336 GB of raw FFT data acquired over a cumulative time of 292 h. During this period the furnace temperature exhibited drift which ranged from -8 to -18 mK/day. This drift created most of the slight separations in the data points within the upper and lower sections of the 3 K interval. The separation between the upper and lower sections was, however, a

Table I. Uncorrected Data Summary Based on Noise Temperatures Derived From the Three-Parameter Model

T_{90} (K)	$u(T_{90})$ (mK)	a_0	$u(a_0)$ (10^{-6})	$T - T_{90}$ (mK)	$u(T)$ (mK)	$T - T_{90}/T_{90}$ (10^{-6})	$u(\Delta T/T_{90})$ (10^{-6})
690.625	6	1.013081	48	−10	32	−15	47
690.533	4	1.012915	47	−20	32	−29	47
690.508	4	0.999949	45	−49	31	−71	45
690.510	5	1.000002	50	−16	35	−23	50
690.488	7	0.999968	38	−16	26	−23	38
690.423	2	0.999817	64	−49	44	−71	64
690.390	4	0.999777	44	−44	30	−64	44
693.239	6	1.004621	41	−58	28	−83	41
693.169	4	1.004583	48	−10	33	−15	48
693.154	3	1.004649	47	51	33	74	47
693.140	3	1.004580	47	19	32	28	46
693.124	3	1.004512	47	−10	32	−15	47
693.027	3	1.004268	48	−72	33	−104	47
692.941	3	1.004174	43	−39	29	−57	43
692.934	3	1.004205	49	−12	34	−18	48
692.887	2	1.004084	49	−45	34	−65	49
692.876	1	1.004161	47	18	32	26	46
692.864	2	1.004085	43	−27	30	−39	43
692.832	2	1.004092	43	8	30	11	43
692.821	2	1.004033	43	−21	29	−31	42
Weighted average, pooled standard deviations				−20	32	−29	46
Standard deviation of the mean					7		10.4

result of a deliberate resetting of the furnace control set points. The furnace drift was also responsible for most of the statistical variance in T_{90} listed in Table I.

4. CORRECTIONS

The results of Table I are subject to several small corrections, two of which require an accurate equivalent circuit model of the coupling network, and in one case, a knowledge of $T - T_{90}$ via other experiments. All the data presented here are subject to the same corrections which are summarized in Table II and discussed below.

4.1. Reference Temperature

The reference probe is equilibrated in the water bath to one of several fixed temperatures in the range $308\,\mathrm{K} < T_2 < 314\,\mathrm{K}$ depending on

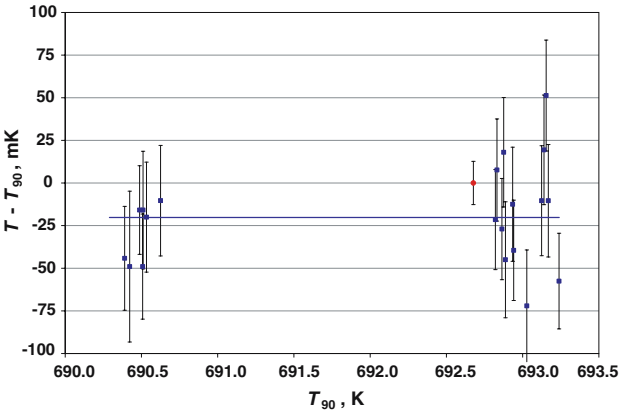

Fig. 5. Difference between the inferred noise temperature T as derived from the three-parameter fits and T_{90} form SPRTs. The data is uncorrected and error bars represent $k = 1$ type A uncertainties only. The weighted mean is shown as a horizontal line at -20 mK. The ITS-90 value is shown for the Zn freezing point with its estimated $k = 1$ uncertainty [8].

Table II. Corrections in Relative Values and in mK

	$\mu K \cdot K^{-1}$	mK
Reference temperature	13	9
Gate resistor attenuation	−14	−9
Gate resistor noise	10	6
Net correction	9	6
	$T - T_{90}/T_{90}$	$T - T_{90}$ (mK)
Raw weighted mean:	−29	−20
Corrected result	−20	−14

experimental requirements. These temperatures are given by the capsule SPRT as calibrated on the ITS-90. Results from various acoustic resonance gas thermometers since 1999 now indicate that the ITS-90 is in error by $T - T_{90} = +4$ mK or $T - T_{90}/T_{90} = +13\,\mu K \cdot K^{-1}$ in this region of temperature [12]. This results in a correction of +9 mK at $T_1 \cong 692$ K.

4.2. Gate Resistors

The junction field effect transistor (JFET) pre-amplifier used for this work is capacitively coupled at the input, which necessitates the use of

large value "gate resistors" $R_g = 20\,\mathrm{M\Omega}$ to allow a path to ground for the $\approx 1\,\mathrm{pA}$ of gate leakage current of each JFET [13]. These gate resistors create a frequency-independent attenuation in the actual voltage being amplified by each JFET depending on the value of the source resistance. This results in an error in the a_0 parameter of the measured power ratio spectrum of $4(R_2 - R_1)/R_g = +14\,\mu\mathrm{K}\cdot\mathrm{K}^{-1}$ where $R_1 = 56.5\,\Omega$ for our Pt–W alloy resistor elements at 693 K and $R_2 = 125.2\,\Omega$. However, when the effect of the correlated noise of the gate resistors is included, an additional error term must be added of $(2T_g/R_g)(R_1/T_1 - R_2/T_2) \approx -10\,\mu\mathrm{K}\cdot\mathrm{K}^{-1}$ where $T_g \approx 298\,\mathrm{K}$. This results in a net error due to the gate resistors of only $+4\,\mu\mathrm{K}\cdot\mathrm{K}^{-1}$, and a correction of $-4\,\mu\mathrm{K}\cdot\mathrm{K}^{-1}$ or $-3\,\mathrm{mK}$ is applied to the data.

5. UNCERTAINTIES

A summary of the estimated uncertainties is given in Table III. The combined standard uncertainty of $35\,\mu\mathrm{K}\cdot\mathrm{K}^{-1}$ or 24 mK is the root-sum-square of all estimated uncertainty components. The individual line items are all standard uncertainties and are discussed below.

5.1. Statistics

The statistical uncertainties are based on standard error estimates for a_0 for each individual fit. The prediction for statistical precision from Eq. (3) is based on the standard deviation of the mean for a single estimator of a single noise spectrum. As an example, for a moderate length run of

Table III. Summary of Estimated Standard Uncertainties for the Noise Temperature T_1

	$\mu\,\mathrm{K}\cdot\mathrm{K}^{-1}$	mK
Statistics (Std. Dev. mean)	10	7
Spectral model	16	11
EMI	28	19
Nonlinearity[a]	2	1.4
Reference temperature	5	3
T_2 correction	2	1
Resistance ratio	3	2
Gate resistor correction	2	1.4
RSS	35	24

[a] $\eta = 0.33\%$.

18 h, each of the two inputs produce a spectrum for which $t_{\text{int}} = 8.6$ h per input once dead time is subtracted out. The ratio of total input noise to correlated noise is $(S_C + S_N)/S_C = 1.24$ for these data. Since we normally include data well beyond the 3 dB point (200 kHz) of the digital filter, the statistics are limited by the correlation bandwidth $\Delta f_c = 265$ kHz of the filter response. Application of Eq. (3) then yields the relative uncertainty $u_r(S_1/S_2) = (u_r^2(S_1) + u_r^2(S_2))^{1/2} = 18\,\mu\text{K}\cdot\text{K}^{-1}$ for the uncertainty of a single estimator for the ratio spectrum.

With multiple parameters fitted to each ratio spectrum, however, the uncertainty $u_r(a_0)$ will always be greater than this single parameter (e.g., simple mean) uncertainty. For a data run of this length, we typically achieve $u_r(a_0) \cong 22$, 43, and $57\,\mu\text{K}\cdot\text{K}^{-1}$, for two-parameter, three-parameter, and four-parameter fits, respectively. The pooled value for the standard deviations of the three-parameter fits is 32 mK as shown in the second-to-last row of Table I. This value is then divided by $\sqrt{20}$ to obtain 7 mK, or $10\,\mu\text{K}\cdot\text{K}^{-1}$, for the standard deviation of the mean as shown in the last line of Table I. This value is used for the Type A standard uncertainty estimate in the first row of Table III.

5.2. Spectral Model

There is uncertainty from the spectral fitting model because it may not necessarily be adequate to find the true asymptotic value for S_1/S_2. The model is physically motivated in the sense that quadratic terms in f will always be associated with RC and $\sqrt{LC}$ time constants, while dielectric loss will give rise to linear terms such as $4\pi f RC \tan\delta$. However, it is generally not known exactly which capacitances are exhibiting the loss that is manifest as linear dependence in the spectra. It is even possible to produce ratio spectra which appear predominately linear out to 450 kHz by utilizing the capacitive compensation methods described above. However, $\tan\delta$ itself is often frequency dependent which obscures the physical significance of any such apparent linear dependence.

The two-parameter fits often exhibit some structure in the residuals, and obviously fail when the inputs are well-compensated producing relatively flat ratio spectra. While the statistical measures derived from the residuals of the fits generally improve slightly as the order of the polynomial increases, even simple cubic fits (four parameters) can produce curvature in the low-frequency end of the spectrum which sometimes appears unphysical. The average value for $a_0 - a_{90}$ is $90\,\mu\text{K}\cdot\text{K}^{-1}$ (or roughly two standard uncertainties) higher for the two-parameter fits than from that of the three-parameter fits. In contrast, the average $a_0 - a_{90}$ values for the three-parameter and four-parameter fits are only $6\,\mu\text{K}\cdot\text{K}^{-1}$ apart. Hence,

there are both physical and statistical reasons for using only three parameters to model the relative frequency dependence of the ratio spectra.

Given these considerations, we base our inferred noise temperatures on the three-parameter fitting model, but include a type B uncertainty estimate of σ_{Mod} to account for its possible inadequacies. The estimate is derived by comparing the a_0 values from the three-parameter fits with simple 50 kHz wide mean values taken over the low end of the spectra. The average of the differences between these two statistics is $28\,\mu\mathrm{K}\cdot\mathrm{K}^{-1}$, which we treat as the half-width of a rectangular distribution so that $\sigma_{\mathrm{Mod}} = 16\,\mu\mathrm{K}\cdot\mathrm{K}^{-1}$.

5.3. Periodic Interference

The existence of electromagnetic interference (EMI) is always a possibility in JNT systems. We take some normal precautions by avoiding the use of switching power supplies whenever possible, and decoupling the outputs of those which we do use. We also take steps to remove the electronics from the near fields of any fans or motors. Nonetheless, we do observe several low-frequency interference lines in both our single-input and ratio spectra. Since these lines are all below 500 Hz, they are not included in the averaged frequency bins which start at 1 kHz in our noise ratio spectra. We likewise do not observe harmonics of the line voltage ($n \times 60$ Hz) beyond $n = 3$. It is possible, however, for any such higher harmonics to be smeared out into a quasi-continuous spectra over time due to frequency instabilities in the power utility [14]. While our local 60 Hz oscillator is stable to within ± 0.01 Hz, all other sources of 60 Hz fields in our building remain synchronized with the power utility.

The high-temperature noise probe is generally more susceptible to EMI due to design constraints and its close proximity to the high currents circulating in the vacuum furnace heater windings. Our test for EMI involves rotation of the high-temperature noise probe in its thermowell by various rotation angles ϕ over a 270° span. Since most of the interference voltages are induced by coupling to a vector magnetic field [15], this rotation should expose the presence of magnetically coupled EMI in the S_{C} spectra for this noise probe. While these results suggest a periodic EMI effect which is a superposition of $\sin\phi$ and $\sin 2\phi$ coupling, the data are insufficiently precise to extract the amplitudes and rotational phases of this EMI from the thermal noise. We estimate a contribution of $\sigma_{\mathrm{EMI}-1} = 20\,\mu\mathrm{K}\cdot\mathrm{K}^{-1}$ as derived from the differences observed in the $a_0 - a_{90}$ values from the rotational coupling experiments of our high-temperature noise probe. In addition, we estimate other contributions from possible axial fields coupling to the high-temperature probe, from fields

coupling to our reference probe, and from other unaccounted-common-mode noise $\sigma_{\mathrm{EMI}-2} = 20\,\mu\mathrm{K}\cdot\mathrm{K}^{-1}$. The total estimated EMI uncertainty is therefore $\sigma_{\mathrm{EMI}} = (\sigma^2_{\mathrm{EMI}-1} + \sigma^2_{\mathrm{EMI}-2})^{1/2} = 28\,\mu\mathrm{K}\cdot\mathrm{K}^{-1}$.

5.4. Nonlinearity

We have used RC compensation to vary the ratio of rms voltage V_i at the two inputs as a test for nonlinearity in the amplifier chain. By adding shunt capacitance to the R_1 input, the effective time constant τ_1 increases, lowering the 3 dB corner frequency of the RC low-pass filter and reducing the noise voltage applied to the pre-amplifier at higher frequencies. This empirical process allows adjustments to be made until the observed power ratio spectrum is "flat" to within $\pm 0.05\%$ of the average value over the entire 1 MHz band. The data shown here are actually generated using variable degrees of compensation such that the parameter $\eta \equiv [V_1^2/V_2^2]^{1/2} - 1$ ranges from -0.1 to 4%. The uncorrected results in terms of $T - T_{90}/T_{90}$ are shown in Fig. 6 versus η. While there is no statistically significant trend in the data, we can not rule out possible effects as large as $25\,\mu\mathrm{K}\cdot\mathrm{K}^{-1}$ for the most unbalanced noise power measurements. We therefore include a type B uncertainty component σ_{NL} to account for possible nonlinearity which varies from 0 to $25\,\mu\mathrm{K}\cdot\mathrm{K}^{-1}$ as η is increased from 0 to 4%.

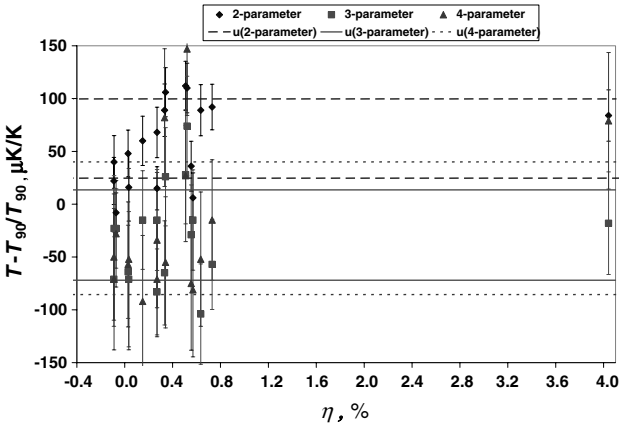

Fig. 6. Results shown in terms of the degree of balance η in the rms input voltages for the three fitting models. The horizontal lines are calculated standard deviations about the means for the three fitting distributions of the fitting parameter a_0.

Table IV. ITS-90 Measurement Uncertainties for SPRTs Used in the Comparison Furnace and Water Bath Systems

	$u(T_{1-90})$ (mK)	$u(T_{2-90})$ (mK)
Statistics	4	1
SPRT calibration	0.25	0.1
WTP stability	3	0.5
Temperature nonuniformity	3	1
Resistance ratios	0.4	0.4
Root-sum-square	5.7	1.5

5.5. ITS-90 Temperatures

The measurement uncertainty of the reference T_2 on the ITS-90, together with the small correction (see Section 4.1 above), contribute directly to our uncertainty in T_1. The measurement uncertainty of T_{1-90}, the furnace temperature on the ITS90, contributes only to the uncertainty of $T - T_{90}$. The individual uncertainty components for both cases are shown in Table IV.

5.6. Probe Resistances

The uncertainty in the ratio R_2/R_1 contributes directly to the uncertainty of T_1. The two resistors are measured separately using the same ac bridge with the same reference resistor, so most systematic effects are unimportant. The base uncertainty in the ac bridge of $2\,\mu\Omega \cdot \Omega^{-1}$ is primarily a linearity specification, from which we derive our estimated uncertainty of $3\,\mu\Omega \cdot \Omega^{-1}$ in the ratio R_2/R_1.

An additional issue to consider is the time constants of the resistances due to parasitic inductances L_{R1}, L_{R2}, and capacitances C_{R1}, C_{R2} which exist within the four-terminal definition of the resistors themselves. These L/R and RC time constants are all <1 ns, and hence are of no practical consequence in comparison to the much larger time constants ($\tau \approx 90$ ns) formed by the parasitic reactances in the input coupling networks N_{ix} and N_{iy}. The remaining caveat is the requirement that the measured resistance at 90 Hz must be equivalent to the real part of the complex impedance Z_1 or Z_2 in the low-frequency limit, or $R(90\,\text{Hz}) = \lim_{f \to 0} \text{Re}[Z(f)]$. This will be satisfied to within the $1\,\mu\Omega^{-1}/\Omega^{-1}$ level for all conceivable combinations of time constants as long as any associated loss tangents $\tan\delta < 3$.

5.7. Insulation Resistance

A closely related issue to that of the above discussion is the finite shunt resistance R_q of the quartz insulators in the high-temperature probe at 693 K. The effects are similar to that of the gate resistors discussed above, except in this case the net resistance of the parallel combination of R_q and R_1 is actually measured *in situ*. This results in an effective error in the inferred noise temperature of $(T_q - T_1)R_1/(T_1 R_q)$ where T_q is the effective temperature of the sections of quartz which are conducting. Our quartz insulators exhibit a finite resistance of $R_q \geqslant 60\,\mathrm{M}\Omega$ at 693 K. So even for $T_q - T_1 \approx -10\%$ of T_1, the error is $< 1\,\mu\mathrm{K}\cdot\mathrm{K}^{-1}$ and can be safely neglected.

6. DISCUSSION

Our present result for the Zn freezing point noise temperature is $T_{\mathrm{ZnFP}} = 692.663 \pm 0.024\,\mathrm{K}$ which can be compared to other similar determinations via noise thermometry found in the literature. Setiawan [16] has determined $T_{\mathrm{ZnFP}} = 692.661 \pm 0.022\,\mathrm{K}$, and de Groot et al. [17] have determined $T_{\mathrm{ZnFP}} = 692.627 \pm 0.037\,\mathrm{K}$. The close agreement of our result with that of Setiawan should be considered fortuitous given the size of the uncertainties.

7. CONCLUSION

Simple resistance-based scaling techniques can be successfully applied in JNT to measure temperatures in the region near 693 K with statistical uncertainties $\approx$32 mK for $\sim$18 h of measurement time. The use of oversampling and digital signal processing can provide information on systematic time constants which allow accurate extrapolation of the power spectral density ratio. We have made comparisons of JNT-based temperatures with the ITS-90 in the immediate region of the Zn freezing point obtaining $T - T_{90} = -14 \pm 24\,\mathrm{mK}$. The results are consistent with the ITS-90, other JNT determinations, and the archival gas thermometry data sets at this temperature.

The present measurement uncertainty is limited by EMI effects for which we can presently only estimate the magnitude. Since the true extent of these and other systematic effects have not been fully investigated, our results for $T - T_{90}$ should be considered preliminary. It should be possible to reduce the overall uncertainty by a factor of $\approx$2 by reduction of EMI contributions and continued refinement of these techniques. A fundamental test of the theoretical basis of JNT is also possible by

comparing results from the resistance-based scaling methods presented here with new methods now under development. Those relative-noise-power-scaling methods employ the quantized voltage noise source [7,8] which allows effective cancellation of all time constants which are not temperature dependent.

ACKNOWLEDGMENTS

The authors wish to acknowledge the innovative electronics design work and conceptual foundations contributed by John Martinis of the Physics Department of the University of California, Santa Barbara. D. Rod White of the New Zealand Measurements Standards Laboratory, Industrial Research, Ltd. has provided important design and theoretical contributions. Dean Ripple of the NIST Process Measurements Division provided many helpful suggestions and comments during the course of this work. We also thank Greg Strouse and Dennis Minor of the Process Measurements Division for providing the ITS-90 calibrations.

REFERENCES

1. H. Preston-Thomas, *Metrologia* **27**:3 (1990); *Metrologia* **27**:107 (erratum).
2. G. F. Strouse, D. R. Defibaugh, M. R. Moldover, and D. C. Ripple, in *Temperature: Its Measurement and Control in Science and Industry*, Vol. VII, D. C. Ripple, ed. (American Institute of Physics, New York, 2003), pp. 31–36.
3. D. R. Taubert, J. Hartmann, J. Hollandt, and J. Fischer, in *Temperature: Its Measurement and Control in Science and Industry*, Vol. VII, D. C. Ripple, ed. (American Institute of Physics, New York, 2003), pp. 7–12.
4. D. R.White, R. Galleano, A. Actis, H. Brixy, M. de Groot, J. Dubbeldam, A. Reesink, F. Edler, H. Sakurai, R. L. Shepard, and J. C. Gallop, *Metrologia* **33**:325 (1996).
5. J. R. Labenski, W. L. Tew, S. W. Nam, S. P. Benz, P. D. Dresselhaus, and C. J. Burroughs, *IEEE Trans. Instrum. Meas*. **56**:481 (2007).
6. D. R. White, *IEEE Trans. Instrum. Meas*. **IM-38**:1036 (1989).
7. R. L. Rusby, R. P. Hudson, M. Durieux, J. F. Schooley, P. P. M. Steur, and C. A. Swenson, *Metrologia* **28**:9 (1991).
8. S. Nam, S. Benz, P. Dresselhaus, W. L. Tew, D. R. White, and J. M. Martinis, *IEEE Trans. Instrum. Meas*. **52**:550 (2003).
9. S. W. Nam, S. P. Benz, P. Dresselhaus, C. J. Burroughs, W. L. Tew, D. R. White, and J. M. Martinis, *IEEE Trans. Instrum. Meas*. **54**:653 (2005).
10. B. W. Mangum and G. T. Furukawa, *NIST Tech. Note 1265* (1990).
11. G. F. Strouse, in *Temperature: Its Measurement and Control in Science and Industry*, Vol. VI, J. F. Schooley, ed. (American Institute of Physics, New York, 1993), pp. 169–174.
12. R. Rusby, M. R. Moldover, J. Fischer, D. R. White, P. P. M. Steur, R. P. Hudson, M. Durieux, and K. D. Hill, *Consultative Committee on Thermometry, CCT/05–19*, BIPM, Sevres, France (2005).
13. D. R. White and E. Zimmermann, *Metrologia* **37**:11 (2000).

14. D. R. White, R. S. Mason, and P. Saunders, *Proc. Tempmeko 2001*, B. Fellmuth, J. Seidel, and G. Scholz, eds. (VDE Verlag, Berlin, 2002), pp. 129–134.
15. D. R. White, *Proc. Tempmeko 2004*, D. Zvizdic, ed. (LPM and FSB, University of Zagreb, Croatia, 2005), pp. 485–490.
16. W. Setiawan, *Systematische Untersuchung von Fehlerquellen bei der Prazisionsrauschthermometrie*, Ph. D. Dissertation (Forschungszentrum Jülich, Germany, 1992).
17. M. de Groot, J. F. Dubbeldam, H. Brixy, F. Edler, and E. Tegeler, *Consultative Committee on Thermometry Report, CCT/96–30*, BIPM, Sevres, France (1996).